

# State of the art on nuclear heating measurement methods and expected improvements in zero power research reactors

Mael Le Guillou\*, Adrien Gruel, Christophe Destouches, and Patrick Blaise

CEA, DEN/DER/SPEX, Centre de Cadarache, F-13108 Saint-Paul-lez-Durance Cedex, France

Received: 9 September 2016 / Received in final form: 15 December 2016 / Accepted: 25 January 2017

**Abstract.** The paper focuses on the recent methodological advances suitable for nuclear heating measurements in zero power research reactors. This bibliographical work is part of an experimental approach currently in progress at CEA Cadarache, aiming at optimizing photon heating measurements in low-power research reactors. It provides an overview of the application fields of the most widely used detectors, namely thermoluminescent dosimeters (TLDs) and optically stimulated luminescent dosimeters. Starting from the methodology currently implemented at CEA, the expected improvements relate to the experimental determination of the neutron component, which is a key point conditioning the accuracy of photon heating measurements in mixed  $n$ - $\gamma$  field. A recently developed methodology based on the use of  ${}^7\text{Li}$  and  ${}^6\text{Li}$ -enriched TLDs, precalibrated both in photon and neutron fields, is a promising approach to deconvolute the two components of nuclear heating. We also investigate the different methods of optical fiber dosimetry, with a view to assess the feasibility of online photon heating measurements, whose primary benefit is to overcome constraints related to the withdrawal of dosimeters from the reactor immediately after irradiation. Moreover, a fibered setup could allow measuring the instantaneous dose rate during irradiation, as well as the delayed photon dose after reactor shutdown. Some insights from potential further developments are given. Obviously, any improvement of the technique has to lead to a measurement uncertainty at least equal to that of the currently used methodology ( $\sim 5\%$  at  $1\sigma$ ).

## 1 Technical background and issues of nuclear heating measurements

As part of the development of the nuclear technology, the accurate determination of nuclear heating of materials is a major issue of the design studies for future power and research reactors (structural design, materials evolution, components lifespan, etc.). The technical choices resulting from this issue directly condition the technological characteristics of nuclear systems, both in terms of safety and performance. The validation of neutron and photon calculation schemes related to nuclear heating prediction, in terms of codes (MCNP, TRIPOLI) and associated nuclear data libraries (ENDF, JEFF), are strongly dependent on the implementation of nuclear heating measurements. Such measurements are usually performed in very low-power reactors (ZPRs), whose core dimensions are accurately known and where irradiation conditions (power, flux, temperature, etc.) are entirely controlled. As shown in Figure 1, nuclear heating arises from the local deposition of energy carried by neutrons, prompt photons issued from fission, radiative capture and inelastic neutron

scattering, and delayed photons emitted by fission and activation products decay. This energy is transferred to the electrons through neutral particle interactions, and finally deposited in the material. In ZPR, the very low operating power (typically of the order of 100 W) does not allow nuclear heating to be directly determined in  $\text{W g}^{-1}$  through temperature measurement (calorimetry) [1,2]. Thus, experimental techniques usually used for this kind of measurements, such as photographic films, semiconductor diodes, luminescent dosimeters, etc., are based on the quantification of the energy deposited per unit mass (absorbed dose) in the material of interest subjected to ionizing radiation (photons, neutrons, charged particles). Hence the thickness of surrounding material in which nuclear heating is measured must be sufficient to reach the charged particles equilibrium (CPE) in the detectors [3]. Ionization chambers can also be used for flux measurements [4]. Among these techniques, two are particularly suitable for photon heating measurements in ZPR, since they do not depend on the photon energy over the reactor photon spectrum (see Fig. 7 in Sect. 3.3):

– Thermoluminescent dosimetry (TLD) [5], illustrated in Figure 2 [6], exploits the ability of some crystalline materials to trap electrons excited through ionizing radiation at intermediate energy levels induced between

\* e-mail: [mael.leguillou@gmail.com](mailto:mael.leguillou@gmail.com)

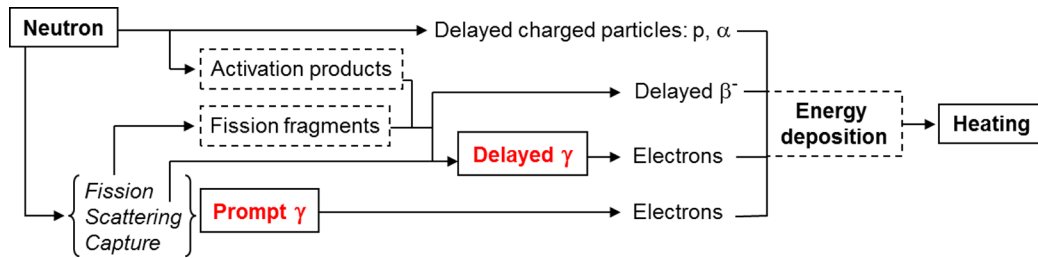


Fig. 1. Simplified view of nuclear heating mechanisms [6].

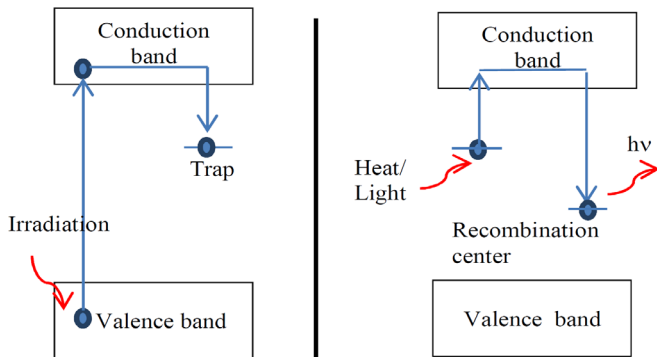


Fig. 2. Principle of TLD and OSLD detection methods [6].

their valence and conduction bands by pristine or artificial defects in their structure (vacancies, dislocations, chemical impurities). Electrons trapped in the gap are then released through post-irradiation thermal stimulation (furnace) according to a heating law specifically optimized for each type of TLD dosimeters (heating rate, temperature, duration). Meanwhile, the luminescence emitted by radiative recombination of some released electrons is collected by a photomultiplier tube (PMT) and converted into absorbed dose thanks to calibration and correction factors. TLDs are reusable after thermal annealing.

- Optically stimulated luminescent dosimetry (OSLD) [7] is based on the same principle as TLD (see Fig. 2), except that trapped electrons are released through optical stimulation (light flash from a laser or LED). The incident light is filtered prior to collection of the luminescence by the PMT. The optical stimulation is perfectly controlled in terms of intensity and duration. Thus, it can release only a very small proportion of trapped electrons, so that, unlike for TLDs, it is possible to read OSLDs several times after each measurement. They are also reusable for further measurements without annealing step. It is noticeable that some materials such as alumina simultaneously exhibit TL and OSL properties.

The following sections are dedicated to the use of TLD/OSLD techniques, as a first step from the point of view of the various application fields in which they are implemented, then in the frame of the nuclear heating measurement methodology developed at CEA Cadarache, and finally, with a view to explore the potential improvement opportunities given by the optical fiber dosimetry for online heating measurements. It is important to notice that the term

“photon heating”, which is used throughout this article, refers in our case to the measured or calculated photon doses, and not to an actual temperature rise strictly speaking.

## 2 Luminescent dosimetry techniques: overview of application fields

### 2.1 General comments

In a general way, whatever the field of applications in which they are implemented, TLD and OSLD techniques should fulfill the following experimental requirements [8]:

- high dynamics, i.e., wide linearity range of dosimeter luminescent response as a function of absorbed dose, generally limited by a supralinear zone preceding the saturation at high doses;
- high sensitivity, i.e., strong luminescent signal per unit of absorbed dose, particularly crucial in medical and personal dosimetry (see Sects. 2.2 and 2.3);
- high selectivity, i.e., sensitivity to the suitable ionizing radiation in the considered application field (photon, neutron, charged particles);
- low dependency on the radiation energy and dose rate;
- low fading, i.e., low signal decay in the thermal and optical conditions in which dosimeters are stored between irradiation and readout steps;
- simplicity of the luminescent signal for an optimized thermal/optical stimulation protocol, allowing an easy further processing of the results;
- spectral accordance between the luminescent emission and the sensitive range of the PMT;
- physical and chemical properties suitable for the measurement environment (mechanical strength, chemical inertness, radiation-resistance, etc.).

In practice however, it is relatively difficult to gather all these requirements within the same experimental setup. Consequently, the choice of the detector characteristics strongly depends on the application field in which it is used.

### 2.2 Medical physics

TLD and OSLD techniques are widely developed in medical physics for the detection of many types of radiation ( $\alpha$ ,  $\beta$ , neutron,  $\gamma$ ,  $X$ ), both in the field of diagnostic (radiology, medical imaging) and for the monitoring of tumor and cancer treatments (radiotherapy, BNCT<sup>1</sup>, etc.) [9,10]. Medical applications make use of

<sup>1</sup> Boron Neutron Capture Therapy.

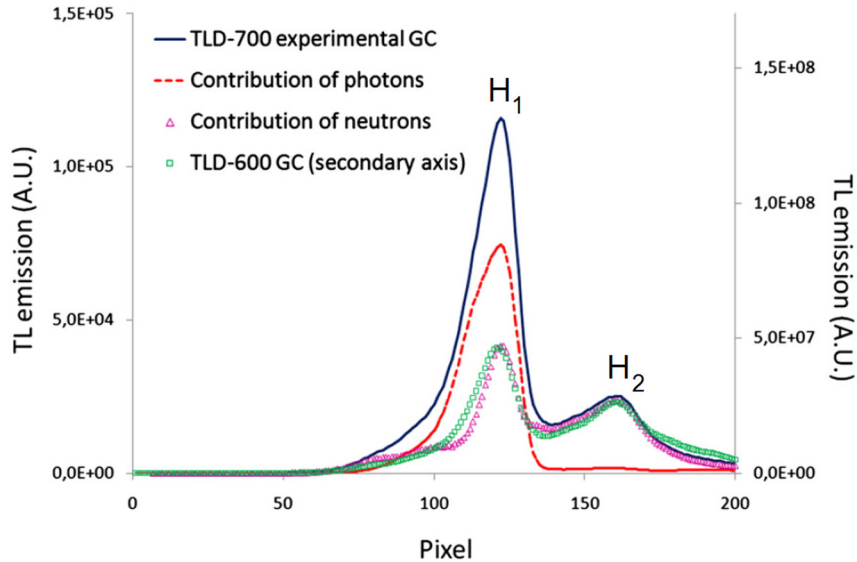


**Fig. 3.** Contributions of photons (red dashes) and neutrons (pink triangles) to the glow curve (GC) of a TLD-700 ( ${}^6\text{Li}/{}^7\text{Li} \sim 0.01\%$ ) irradiated in mixed  $n\text{-}\gamma$  field (blue line), compared with the glow curve of a TLD-600 ( ${}^6\text{Li}/{}^7\text{Li} \sim 95.6\%$ ) irradiated with thermal neutrons (green squares, secondary axis) [11].

many luminescent materials, such as doped lithium fluoride (LiF:Mg,Ti, LiF:Mg,Cu,P), doped calcium fluoride (CaF<sub>2</sub>:Dy, CaF<sub>2</sub>:Tm, CaF<sub>2</sub>:Mn) or doped alumina (Al<sub>2</sub>O<sub>3</sub>:C), whose dosimetric properties, in terms of repeatability, reproducibility, sensitivity, fading, energy dependence, spectral emission, etc., are being studied for decades along with their experimental implementation (annealing and heating laws, signal processing, online measurements). Historically, the most commonly used dosimeters for such applications are LiF-based TLDs, whose effective atomic number ( $Z_{\text{eff}}=8.2$ ) is close to that of human tissues (around 7–8). These TLDs are usually synthesized in the form of powders or solid pellets with natural lithium for measurements in pure  $\gamma$  field. For measurements in mixed  $n\text{-}\gamma$  field, they are enriched with  ${}^6\text{Li}$  (resp.  ${}^7\text{Li}$ ) so as to increase (resp. decrease) their neutron sensitivity thanks to the (n,T) activation reaction on  ${}^6\text{Li}$  in the thermal field. Since the photon sensitivity of  ${}^6\text{Li}$  and  ${}^7\text{Li}$ -enriched TLDs are equivalent, and assuming that their isotopic composition is accurately known, differential measurements with these two types of TLDs could allow estimating both the neutron and photon doses in a mixed field. Researchers from INFN<sup>2</sup> recently proposed a method for determining the photon dose and the thermal neutron fluence in a BNCT  $n\text{-}\gamma$  field from the glow curves (GCs) of LiF TLDs [11]. This method, illustrated in Figure 3, relies on the deconvolution of the signal of a TLD-700 ( ${}^7\text{Li}$ -enriched, low neutron sensitivity) irradiated in mixed field, using the GCs obtained from the same TLD irradiated in a pure  $\gamma$  field (photon calibration), and with thermal neutrons (neutron calibration). It makes the assumption that, after background noise subtraction, the heights  $H_1$  and  $H_2$  of the two peaks exhibited by the TLD-700 GC in mixed  $n\text{-}\gamma$  field can be related to the absorbed photon dose  $D_\gamma$  and

the thermal neutron fluence  $\phi_n$  through expressions (1) and (2):

$$H_1 = D_\gamma H_1^\gamma + \phi_n H_1^n, \quad (1)$$

$$H_2 = D_\gamma H_2^\gamma + \phi_n H_2^n, \quad (2)$$

where  $H_1^\gamma$ ,  $H_1^n$ ,  $H_2^\gamma$  and  $H_2^n$  correspond to the respective heights of photon ( $\gamma$ ) and neutron ( $n$ ) contributions to the first (subscript 1) and the second (subscript 2) peaks of the TLD-700 GC, normalized to dose and fluence units. Hence the photon and neutron contributions to the total absorbed dose are given by equations (3) and (4), respectively:

$$D_\gamma = \frac{H_2 R_n - H_1}{H_2^\gamma R_n - H_1^\gamma} \text{ where } R_n = \frac{H_1^n}{H_2^n}, \quad (3)$$

$$\phi_n = \frac{H_2 R_\gamma - H_1}{H_2^n R_\gamma - H_1^n} \text{ where } R_\gamma = \frac{H_1^\gamma}{H_2^\gamma}. \quad (4)$$

The  $R_\gamma$  ratio is obtained from the TLD-700 calibration in a pure  $\gamma$  field, and the  $R_n$  ratio from the GC of an uncalibrated TLD-600 irradiated with thermal neutrons, assuming that the photon contribution for this latter type of TLD is usually negligible due to the 95.6%  ${}^6\text{Li}$  enrichment. The peak heights  $H_1^\gamma$  and  $H_2^\gamma$  are deduced from the TLD-700 photon calibration and normalized to dose unit, while  $H_1^n$  and  $H_2^n$  are obtained from the TLD-700 thermal neutron calibration and normalized to fluence unit. The accuracy of this method can be tested by comparing the neutron component obtained through photon dose subtraction, calculated with equation (3) from the TLD-700 GC obtained in mixed  $n\text{-}\gamma$  field, with the GC of a TLD-600 irradiated with thermal neutrons. As shown in Figure 3, the neutron component of the TLD-700 response (pink triangles) and the TLD-600 GC (green squares) are in rather good agreement.

<sup>2</sup> Istituto Nazionale di Fisica Nucleare (Milan, Italy).

### 2.3 Personal and environmental dosimetry

The radiological monitoring of workers exposed to ionizing radiation, as well as of nuclear facilities environment, relies inter alia on the luminescent dosimetry techniques. Because of their dosimetric properties (repeatability, sensitivity, etc.), some materials such as LiF:Mg,Cu,P and Al<sub>2</sub>O<sub>3</sub>:C are particularly suitable for extremity monitoring and for very low-level dosimetry in the environment. Generally, the commonly used dosimeters simultaneously exhibit the sensitivity and dynamic properties (linearity range) required for medical physics applications and personal/environmental dosimetry. Tables 1 and 2 synthesize some characteristics of the most widely used dosimeters within these application fields [8,9,12–23]. The reported values are taken from the performance specifications provided by manufacturers, as well as from experimental data available in the literature. The corresponding uncertainties are not specified in these tables in order to clarify the reading (see references for more detailed information).

### 2.4 Space applications

Dosimetry in space environment has been developed in view to quantify the radiation effects suffered by on-board electronic systems embedded in remote sensing and telecommunication satellites, navigation systems (GPS), scientific devices (such as Hubble telescope) or manned space flights to ISS. The electronic components launched at altitudes ranging from about 2000 km to beyond 36,000 km (geostationary orbit) are directly subjected to the Van Allen radiation belts, mostly comprised of electrons and protons. Although those components are much more radiation-resistant than living organisms, they are also much more exposed to ionizing radiation than the crews of manned flight (up to some hundreds of km). During the lifetime of a geostationary satellite (of the order of tens of years), its electronic components are likely to be subjected to electron and proton dose rates exceeding 10 mGy min<sup>-1</sup> behind a 3 mm thick aluminum shielding. Such dose rates can lead, after several years, to a drift of the transistors threshold voltages and a deterioration of the current gains in embedded systems. Because of the space flights constraints related to energy consumption, remote readout and compact design, it is not possible to use TLDs as on-board dosimeter system. However, the OSLD technique provides the sensitivity and dynamic properties and the remote measurement opportunities suitable for embedded components monitoring, in addition to the currently used techniques (integrators measuring the transistors drift, particle counting systems, etc.). Feasibility studies have been carried out at IES<sup>3</sup> with the aim to set up a dose mapping technique for both particle beam characterization and embedded dosimetry in harsh environments. They have led to the development of a compact OSL system with a sensitivity of a few tens of mGy, based on alkaline earth sulfides from Lenard's family (MgS, CaS, SrS, BaS) doped with rare earths (Ce, Sm) and boron [24,25]. These materials exhibit the operating properties

<sup>3</sup> Institut d'Électronique et des Systèmes (formerly Institut d'Électronique du Sud, Montpellier, France).

**Table 1.** Dosimetric properties of the most commonly used dosimeters in medical physics and personal dosimetry [8,9,12–23].

Mat.	Z <sub>eff</sub>	Doping	Dosimeter <sup>a</sup>	[ <sup>6</sup> Li]	Linearity range <sup>b</sup>	Repeatability	Uniformity (batch, lot)	Fading	Relative sensitivity		Applications		
									/TLD-100	n <sub>th</sub> /γ			
<sup>nat</sup> LiF	8.2	Mg,Ti	TLD-100	7.5% [9] 7.36% [12]	10 <sup>-5</sup> -10 Gy [8,13]	<2% [13]	7.5% [13]	5% y <sup>-1</sup> [13] 5-10% y <sup>-1</sup> [8] <5% an <sup>-1</sup> [14] <5% y <sup>-1</sup> [15]	1 [13]	1 [13]	Medical physics		
			MTS-N		5 × 10 <sup>-5</sup> -5 Gy [14]	<2% [14]	<5% [14]		1.5 [14]				
			GR-100		10 <sup>-7</sup> -12 Gy [15]								
			TLD-100H		10 <sup>-6</sup> -10 Gy [13] 10 <sup>-6</sup> -20 Gy [8]				Negl. [13] 3% y <sup>-1</sup> [8]	15 [13]			γ, β dosimetry personal, environment
<sup>6</sup> LiF	8.2	Mg,Cu,P	MCP-N		10 <sup>-7</sup> -10 Gy [14]	<2% [14]	<5% [14]	<5% y <sup>-1</sup> [14]	40 [14]				
			MCP-Ns		10 <sup>-6</sup> -10 Gy [14]	<2% [14]		<5% y <sup>-1</sup> [14]	1 [14]				
			GR-200		10 <sup>-7</sup> -12 Gy [15]	<2% [15]		<5% y <sup>-1</sup> [15]	65 [15]				
			TLD-600		10 <sup>-5</sup> -10 Gy [13] 10 <sup>-5</sup> -20 Gy [8]				5% y <sup>-1</sup> [13] Negl. [8]	1 [13]	350 [16]		Medical physics
			MTS-6		5 × 10 <sup>-5</sup> -5 Gy [14]	<2% [14]	<5% [14]		<5% y <sup>-1</sup> [14]	1.5 [14]			
			TLD-600H		10 <sup>-6</sup> -10 Gy [13] 10 <sup>-6</sup> -20 Gy [8]				negl. [8,13]	15 [13]			Neutron dosimetry personal, environment
MCP-6 MCP-6s GR-206					10 <sup>-7</sup> -10 Gy [14]	<2% [14]	<5% [14]	<5% y <sup>-1</sup> [14]	40 [14]				
					10 <sup>-5</sup> -10 Gy [14]	<2% [14]		<5% y <sup>-1</sup> [14]	1 [14]				
					10 <sup>-7</sup> -12 Gy [15]	<2% [15]		<5% y <sup>-1</sup> [15]	192 [16,17]				

<sup>a</sup> TLD-100 to 900 are synthesized by Harshaw (Thermo Fisher Scientific Inc.), MTS and MCP TLDs by TLD Poland, GR TLDs by SDDML (Solid Dosimetric Detector and Method Laboratory), PTL-717 TLDs by Desmarquest-CEC, and nanoDots OSLDs by Landauer.

<sup>b</sup> The luminescent responses of the dosimeters are independent of the dose rate over the considered linearity ranges (up to 1000 MGy s<sup>-1</sup> for Harshaw TLDs).

**Table 2.** Dosimetric properties of the most commonly used dosimeters in medical physics and personal dosimetry [8,9,12–23].

Mat.	$Z_{\text{eff}}$	Doping	Dosimeter <sup>a</sup>	$^{6}\text{Li}$	Linearity range	Repeat.	Uniformity (batch, $1\sigma$ )	Fading	Relative sensitivity		Applications			
									/TLD-100	$n_{\text{th}}/\gamma$				
$^7\text{LiF}$	8.2	Mg,Ti	TLD-700	0.01% [9]	$10^{-5}$ –10 Gy [13]	<2% [13]	7.5% [13]	$5\% \text{ y}^{-1}$ [13]	1 [13]	0.48 [16]	0.07 [18]	$\gamma$ , $\beta$ dosi. medical		
			MTS-7		$5 \times 10^{-5}$ –5 Gy [14]	<2% [14]	<5% [14]	< $5\% \text{ y}^{-1}$ [14]	1.5 [14]					
		Mg,Cu,P	TLD-700H	<0.03% [12]	$10^{-6}$ –10 Gy [13]			Negl. [13]	15 [13]	1.45 [16,17]	0.02 [18]	$\gamma$ , $\beta$ dosi. personal, environment		
			MCP-7		$10^{-7}$ –10 Gy [14]	<2% [14]	<5% [14]	< $5\% \text{ y}^{-1}$ [14]	40 [14]	11.8 [16]				
			MCP-7s		$10^{-5}$ –10 Gy [14]	<2% [14]	<5% $\text{y}^{-1}$ [14]	< $5\% \text{ y}^{-1}$ [14]	1 [14]					
			GR-207	0.007% [19]	$10^{-7}$ –12 Gy [15]	<2% [15]	< $5\% \text{ y}^{-1}$ [15]	< $5\% \text{ y}^{-1}$ [15]			0.95–1.87 [16–17]	0.125 [20]	0.118 [19]	
$\text{Al}_2\text{O}_3$	10.2	C	PTL-717	0.05% [19]										
			TLD-500		$5 \times 10^{-8}$ –1 Gy [13]				$3\% \text{ y}^{-1}$ [8,13]	30 [13]		0.242 [21]	Medical personal, environment	
$\text{CaF}_2$	16.3	Dy	OSLD nanoDot	$10^{-5}$ –3 Gy [22]										
			TLD-200		$10^{-7}$ –10 Gy [8,13]		15% [13]	10% (1 d) [13] 16% (2 wk) [8,13]	30 [13]				Environment	
$\text{Li}_2\text{B}_4\text{O}_7$	7.4	Mn	TLD-300						3 [13]					
			TLD-400		$10^{-7}$ –100 Gy [8,13]		15% [13]	8% (1 d) [13] 12% (3 mth) [13] 15% (3 mth) [8]	10 [13]		0.288 [20] 0.12 [23]	High doses		
$\text{CaSO}_4$	15.5	Dy	TLD-900		$5 \times 10^{-4}$ – $10^5$ Gy [13]			<5% (3 mth) [13]	0.15 [13]		Wide range			
					$10^{-6}$ –100 Gy [13]			2% (1 mth) [13] 8% (6 mth) [13]	20 [13]			Environment		

<sup>a</sup> TLD-200, 500 and 900 are extremely sensitive to UV light, so that they have to be handled and stored away from light sources.

required for the implementation of OSLD technique in space environment: sensitivity to all ionizing radiation, high dynamics, clear spectral separation between optical stimulation and luminescent emission (making easier signal extraction and processing), and rather short readout time with full annealing of electronic traps.

## 2.5 Research reactors

Within nuclear applications, the TLD technique has been used to determine photon heating in many research reactors worldwide. The main experiments during which TLD measurements have been performed are described in detail in references [19,26–37] and briefly summarized below:

- Photon heating measurements were carried out in stainless steel and UO<sub>2</sub> fuel rods of the FBBF<sup>4</sup> fast neutron reactor, using CaF<sub>2</sub> and LiF TLDs encapsulated in stainless steel and lead pillboxes [27]. The measured doses corrected for the fuel background activity are quite consistent between the different types of TLDs. However, the calculation to experiment ratios (C/E), close to 1 in the inner part of the experimental area, decreases to 0.71 in its outer part, and differs from 10 to 15% between steel and lead pillboxes. This highlighted the need to choose a sufficient pillbox thickness to achieve CPE in the TLDs, and to avoid energy deposition from the electrons generated outside the pillbox, especially when its effective atomic number is significantly different from that of the surrounding medium.
- As part of the validation studies on iron nuclear data, photon heating measurements in sodium and stainless steel environments were performed in the BZC/1 sub-assembly of ZEBRA<sup>5</sup> reactor, using LiF TLDs encapsulated in stainless steel pillboxes [28]. The calculation overestimates the measurements (corrected for delayed photon dose) of about 15% (1 $\sigma$ ), that was attributed to the iron nuclear data on photon production through inelastic scattering.
- As part of the validation studies on iron, Teflon and tantalum nuclear data, photon heating was measured in three configurations of the ZPPR<sup>6</sup> core, using LiF TLDs inserted into stainless steel, B<sub>4</sub>C, Teflon and Ta/Na devices [29]. The measured doses were corrected for background noise, delayed photon and neutron components, allowing to achieve C/E ratios ranging from 0.97 in Teflon to 1.03 in B<sub>4</sub>C. This experiment pointed out the need to accurately know the photon spectrum at detectors location so as to properly determine the correction factors to apply to raw measurements.
- Delayed photon dose measurements were performed in the UZrH core of TRIGA II<sup>7</sup> for photon dose rate monitoring after reactor shutdown [30]. LiF powders, beforehand inserted into plastic pillboxes at the center-core of the reactor, were irradiated for 2 h at 250 kW, and

then withdrawn at regular time intervals after shutdown. The delayed gamma doses were averaged over 15 measurements per pillbox with standard deviations ranging from 8 to 15% (1 $\sigma$ ).

- As part of a French-Russian experimental campaign, photon dose measurements in a tissue-equivalent phantom were carried out at 3 m from the core of SILENE<sup>8</sup> reactor, using semiconductor dosimeters and alumina TLDs encapsulated in plastic pillboxes [31]. The uncertainties associated with these measurements were around 5% (1 $\sigma$ ). Moreover, alumina-based detectors were used to measure the photon dose evolution at different distances from the core of CALIBAN reactor, with uncertainties ranging between 0.3 and 11% (1 $\sigma$ ) [32].
- Photon dose measurements were performed in RPI<sup>9</sup> reactor using alumina TLDs to assess the suitability of this type of dosimeters in a mixed *n*- $\gamma$  field [33]. Within an experimental uncertainty of about 6%, the results showed a good agreement with the dose rates measured with a CRGA-11 ionization chamber (stainless steel/nitrogen).
- Photon heating was measured in stainless steel at several locations in the core of VENUS<sup>10</sup> reactor, using LiF, alumina and BeO TLDs with an experimental uncertainty of the order of 10% [34]. Over all the measurement locations, an average C/E ratio of  $1.08 \pm 7.3\%$  (1 $\sigma$ ) was estimated.
- In the frame of RACINE and BALZAC experimental programs conducted in MASURCA<sup>11</sup> critical mock-up, a measurement campaign by LiF TLDs was carried out in order to assess the spatial distribution of photon heating in SFR environments (core, blankets and control rods), with quite large uncertainties (of the order of 25%) [35,36]. Furthermore, during the CIRANO experimental program, performed in MASURCA as part of the CAPRA project, absolute photon heating was measured by LiF TLDs in PuO<sub>2</sub>/UO<sub>2</sub> cores surrounded by a steel/Na reflector, with uncertainties lower than 6% (1 $\sigma$ ) but C/E ratios ranging from 0.84 to 0.90 (underestimation probably due to errors in plutonium and iron nuclear data in core region and reflector respectively) [6,37].

## 3 Photon heating measurements in ZPR: current methodology developed at CEA Cadarache

### 3.1 General comments

At the Experimental Physics Division of CEA Cadarache, the photon heating measurement methodology is

<sup>4</sup> Fast Breeder Blanket Facility (Purdue University, Indiana, US).

<sup>5</sup> Zero Energy Breeder Reactor Assembly (Winfrith, UK).

<sup>6</sup> Zero Power Physics Reactor (formerly Zero Power Plutonium Reactor, Idaho National Laboratory, US).

<sup>7</sup> Training, Research, Isotopes, General Atomics (Vienna, Austria).

<sup>8</sup> Source d'Irradiation à Libre Évolution Neutronique (CEA Valduc, France).

<sup>9</sup> Reactor Português de Investigação (Instituto Tecnológico e Nuclear, Lisbon, Portugal).

<sup>10</sup> Vulcan Experimental Nuclear System (SCK•CEN, Mol, Belgium).

<sup>11</sup> Maquette de Surgénérateur de Cadarache (CEA Cadarache, France).

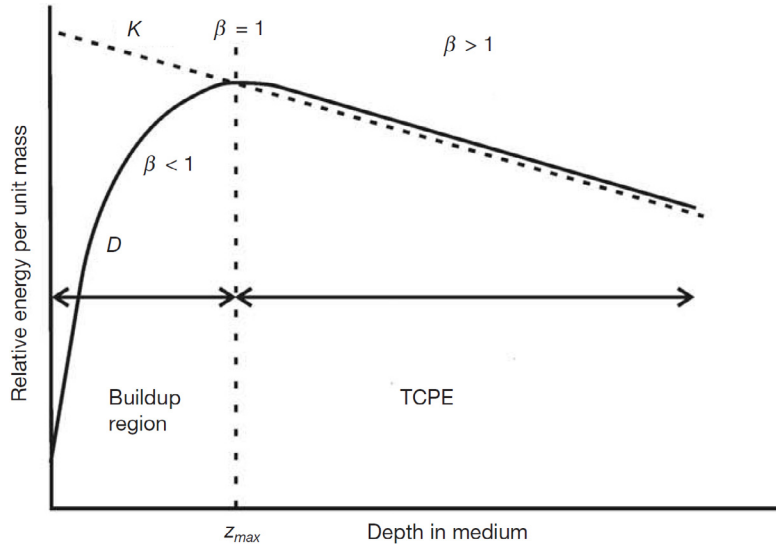


Fig. 4. Kerma and absorbed dose in a medium subjected to high-energy photon flux [45].

implemented in critical mock-ups (ZPRs), whose one is shut down for refurbishment (MASURCA, devoted to fast reactors studies) and two are currently in operation in 2017: – MINERVE: pool type reactor mainly dedicated to validation of nuclear data of fissile isotopes, neutron absorbers and structural materials. – ÉOLE: dedicated to light water reactors studies, including the validation of neutron and photon calculation tools related to the design of future reactors (EPR, JHR<sup>12</sup>, etc.).

As part of the experimental programs conducted in the previous two reactors for more than a decade (ADAPh, ADAPh+, PERLE, AMMON) [6,19,38–44], the successive improvements of the photon heating measurement procedure have led to the currently used methodology, which is described in the following sections. The recent C/E ratios obtained with this methodology range from 0.80 to 1.04 with less than 10% uncertainty ( $1\sigma$ ), depending on the dosimeter types (LiF and CaF<sub>2</sub> TLDs, alumina OSLDs), the pillboxes (plastic, stainless steel, Al, Hf, and Be) and the measurement locations.

### 3.2 Determination of charged particle equilibrium (CPE)

In order to ensure equivalent experimental conditions during both the calibration and the irradiation stages of photon heating measurements, it is required to define the thickness of surrounding material (pillbox) that allows reaching the CPE in the encapsulated dosimeters. This ensures that the deposited energy in the TLDs/OSLDs exclusively comes from particle interactions within the surrounding material in which photon heating is measured (Al, Hf, stainless steel, etc.). The CPE is achieved in a volume subjected to a flow of neutral particles (neutrons,

photons) when the amount of secondary charged particle produced through neutral particle interactions entering this volume is equal to the amount of charged particles leaving it, i.e., when the number of incoming electrons is equal to the number of outgoing electrons. As illustrated in Figure 4, some conditions can lead to a transient charged particle equilibrium (TCPE) beyond a depth  $z_{\max}$  greater than the penetration depth of electrons in the considered medium. Assuming that the radiative interactions (bremsstrahlung, electron-positron annihilation) of secondary charged particles emitted in the volume are negligible with respect to electronic interactions (excitation, ionization), the energy deposited by charged particles in an elementary volume  $dV$  of mass  $dm$ , i.e., the absorbed dose  $D$ , is then directly proportional to the energy transferred by neutral particles in the form of kinetic energy to charged particles in  $dV$ , i.e., the Kerma<sup>13</sup>  $K$  [45,46]. In practice, the  $z_{\max}$  thickness is calculated thanks to Monte Carlo transport codes (MCNP, TRIPOLI) and the associated nuclear data libraries (ENDF, JEFF). An example is given in Figure 5, showing the calculated dose and Kerma in different types of dosimeters irradiated nearby a <sup>60</sup>Co source (Fig. 5a, calibration in  $\gamma$  field) and in the center-core of MINERVE reactor (Fig. 5b, mixed  $n$ - $\gamma$  field), as a function of the aluminum pillbox thickness surrounding the dosimeters. Beyond  $z_{\max}$  (TCPE regime), the proportionality constant  $\beta$  between the Kerma gamma  $K$  and the absorbed dose  $D$ , defined in equation (5), depends on the effective atomic numbers of both the dosimeter and the surrounding material. Thus, equivalent  $Z_{\text{eff}}$  (alumina dosimeter in aluminum pillbox for instance) leads to a quasi-equality between  $K$  and  $D$  [19,46]

$$\beta = \exp(\mu\bar{z}), \quad (5)$$

<sup>12</sup> Jules Horowitz Reactor.

<sup>13</sup> Kinetic energy released per unit mass.

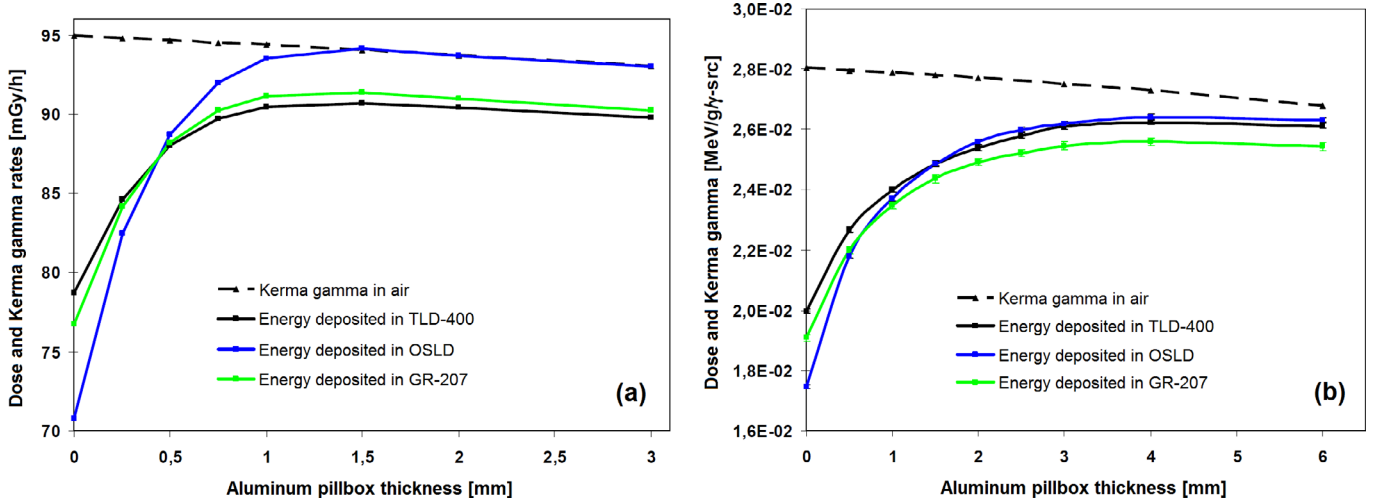


**Fig. 5.** MCNP calculations (with ENDF/B-VI library) run for the determination of TCPE conditions in different types of dosimeters encapsulated in aluminum pillboxes, irradiated nearby a  $^{60}\text{Co}$  calibration source (a) and in the center-core of MINERVE reactor (b) [19].

where  $\mu$  is the linear attenuation coefficient [in  $\text{m}^{-1}$ ] of the photon flux, governing the decreasing slope of  $K$  and  $D$  beyond  $z_{\text{max}}$  (see Fig. 4); and  $\bar{z}$  is the average depth beyond  $z_{\text{max}}$  at which the secondary electrons generated through photon interactions deposit their energy.

It is worth noting that up to  $z_{\text{max}}$  (buildup region),  $K$  overestimates  $D$ , meaning that the secondary electrons produced through neutral particle interactions outside the surrounding material are likely to reach the dosimeter, so that TCPE conditions are not met in the buildup region. Starting from Monte Carlo calculation and considering the constraints related to the instrumentation accessibility in ZPR during the experimental campaigns conducted at CEA Cadarache, the pillboxes encapsulating the TLDs/OSLDs were manufactured with a thickness of 2 mm, sufficient to reach, or at least to approach the TCPE conditions for both calibration and irradiation stages. As shown in Figure 6, the dosimeters are encapsulated in 2 mm thick pillboxes (made of Al, Hf, stainless steel, etc.), on the basis of three different TLDs or OSLDs per pillbox, separated by washers (same composition and thickness as the pillbox) to ensure the isotropy of the cavity in which each dosimeter is inserted.

### 3.3 Calibration in pure $\gamma$ field

In order to establish the relationship shown in equation (6) between the luminescent signal emitted by the dosimeters and a reference quantity representative of the absorbed dose in the pillboxes, TLDs and OSLDs are calibrated in a pure  $\gamma$  field nearby a  $^{60}\text{Co}$  source, whose  $\beta^-$  decay into  $^{60}\text{Ni}$  with a period of about 5.27 years leads to the emission of two gamma rays at 1.17 and 1.33 MeV. This provides the best representativeness conditions with respect to reactor prompt photon spectra illustrated in Figure 7, ranging from 100 keV to 7 MeV with a major contribution to Kerma gamma in air between 1 and 3 MeV, and a mean energy around 1.7 MeV. It is noticeable that the luminescent response of the dosimeters does not depend on the photon

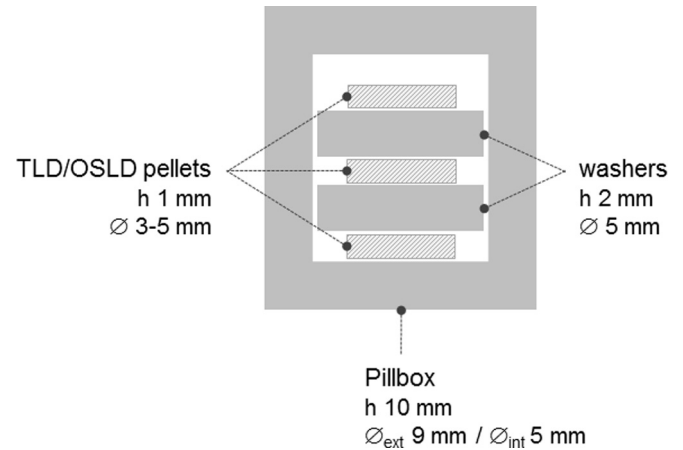


**Fig. 6.** Vertical cross-section of a pillbox encapsulating TLDs/OSLDs and washers.

spectrum over the photon energy range in reactor [19].

$$F_c = \frac{Q_\gamma}{K_{\text{air}}} = \frac{\int I}{K_{\text{air}}}, \quad (6)$$

where  $F_c$  is the calibration factor [in  $\text{nC mGy}^{-1}$  for TLDs, and counts  $\text{mGy}^{-1}$  for OSLDs];  $K_{\text{air}}$  is the reference quantity [in  $\text{mGy}$ ] corresponding to the Kerma gamma in air measured during a time  $\Delta t$  at the calibration location in the absence of dosimeter; and  $Q_\gamma$  is the dosimeter response [in  $\text{nC}$  for TLDs, and counts for OSLDs] corresponding to the integral of the luminescent signal emitted after irradiation during  $\Delta t$ .

$Q_\gamma$  and  $K_{\text{air}}$  are measured at 1 m from the  $^{60}\text{Co}$  source so as to limit the radial variation of the photon flux between the dosimeters encapsulated in the same pillbox, as well as between the different pillboxes within the calibration area. It was calculated that the variation of the photon flux at the location of the different pillboxes does not exceed 0.5% at 1 m from the source within a 5 cm radius around the

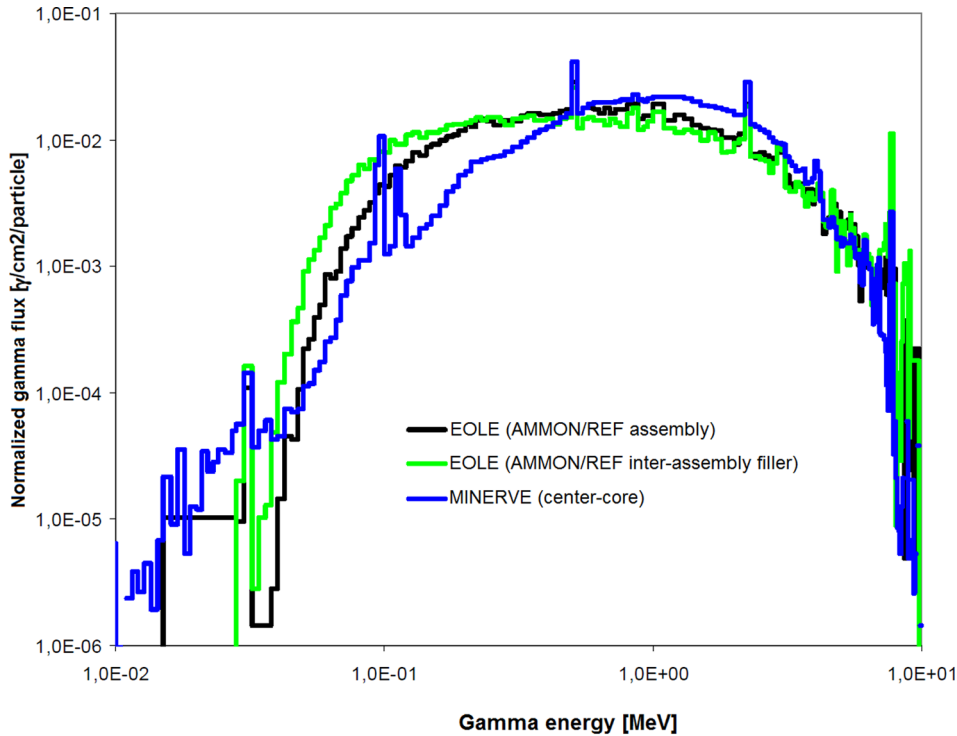


**Fig. 7.** Prompt gamma spectra calculated at two locations in the AMMON/REF core in ÉOLE reactor (TRIPOLI calculations with both JEFF3.1.1 and ENDF/B-VI libraries), and in the center-core of MINERVE reactor (MCNP calculation with ENDF/B-VI library) [19].

incident beam [19]. In addition, it was measured a negligible background noise at this location. The dosimeters are calibrated at different  $K_{\text{air}}$  values between 100 and 1200 mGy by varying their exposure time. That dose range corresponds to the expected one for typical ZPR experiments (low power, irradiation duration of the order of ten minutes to a few hours), and it matches the linearity range of the used dosimeters. Finally, several irradiations are usually performed at each  $K_{\text{air}}$  value in order to assess the repeatability of the measurements. Figure 8 gives an example of calibration curves of TLDs (a) and OSLDs (b) encapsulated in aluminum pillboxes [6,19]. The calibration factor  $F_c$  is deduced from the slope of these curves with less than 5% error ( $1\sigma$ ), taking into account the counting, repeatability and reproducibility uncertainties that depend on the type of dosimeters and the composition of the pillboxes. It is very important to notice that TLDs are calibrated individually because of a significant sensitivity discrepancy (exceeding 5%) within a same batch. OSLDs are batch calibrated since their reproducibility standard deviation does not exceed 2% for a same batch.

### 3.4 Low-power irradiation in mixed $n$ - $\gamma$ field

The irradiation configuration in ZPR measurement channels, illustrated in Figure 9, is based on the stacking of several identical pillboxes encapsulating the same three types of dosimeters into a 0.6 mm thick aluminum or stainless steel guide-tube. The pillboxes stack is centered on the core mid-plane of the reactor thanks to upper

and lower shims, the axial curvature of the neutron and photon fluxes being assumed negligible over the few cm of the stack height. Photon heating measurements in ZPR are performed according to the following methodology [19]:

- photon background noise measurement at the dosimeters locations in the shutdown reactor;
- dose measurement during the divergence of the reactor (drop of the control rods immediately after reaching the desired nominal power), with background noise correction;
- dose measurement during a constant power level (typically 10 min at 10 W), with background noise and divergence dose corrections;
- optionally, delayed photon dose measurement following a higher power irradiation (typically 80 W) up to 30 min after drop of the control rods.

The reproducibility of the measurements is tested by repeating several irradiations in the same experimental conditions, whose power monitoring is ensured by using precalibrated miniature fission chambers ( $^{235}\text{U}$  or  $^{239}\text{Pu}$ ). For an irradiation  $i$ , the total measured dose  $\bar{D}_i$  [in mGy equivalent to  $K_{\text{air}}$  at 1 m from the calibration source, see Sect. 3.3] is defined through equation (7) as the mean of the total doses  $D_j$  measured by the  $n$  dosimeters of the same type encapsulated in the  $n$  pillboxes stacked at the same measurement location [19]:

$$\bar{D}_i = \frac{1}{n} \sum_{j=1}^n D_j = \frac{1}{n} \sum_{j=1}^n \frac{Q_j}{F_c} \times (1 + f), \quad (7)$$

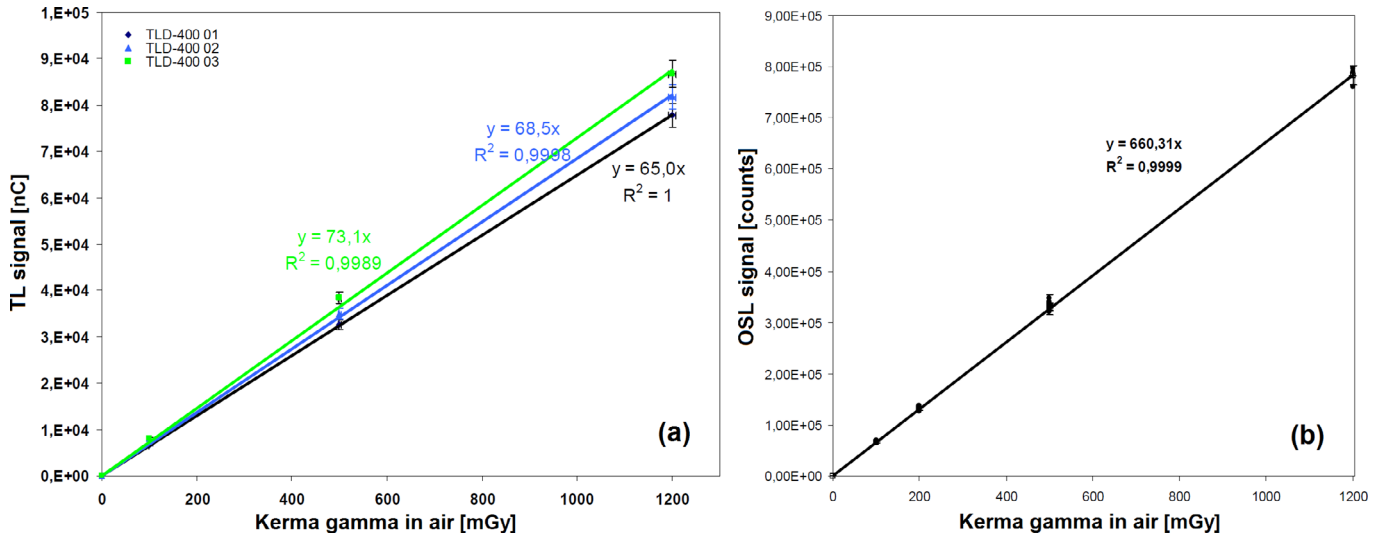


Fig. 8. Calibration curves in pure  $\gamma$  field of TLDs (a) and OSLDs (b) encapsulated in aluminum pillboxes [19].

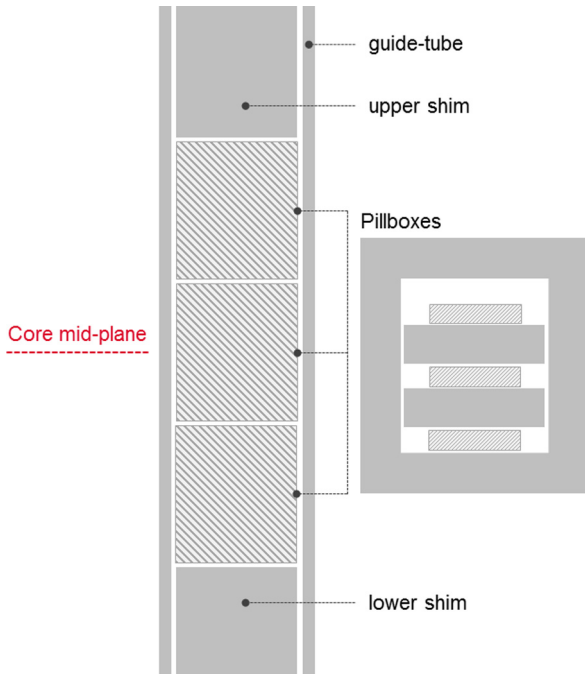


Fig. 9. Irradiation configuration in a ZPR measurement channel.

where  $Q_j$  and  $F_c$  are respectively the luminescent response and the calibration factor of the dosimeter  $j$  (see Sect. 3.3); and  $f$  is the fading coefficient between the end of irradiation and the readout of the dosimeter  $j$ . As far as possible, this time has to be identical during both irradiation and calibration stages. In practice, it is usually about 24 h, the fading being assumed to be negligible ( $f=0$ ) over such duration (see Tabs. 1 and 2, Sect. 2.3).

The uncertainty  $u(\bar{D}_i)$  on the total averaged dose is given by equation (8), where  $u(D_j)$ ,  $u(F_c)$  and  $u(Q_j)$  are the respective uncertainties on  $D_j$ ,  $F_c$  and  $Q_j$  (taking into

account the counting, repeatability and reproducibility uncertainties) [19]:

$$\begin{aligned} u(\bar{D}_i) &= \sqrt{\frac{1}{\sum_{j=1}^n 1/u^2(D_j)}} = \frac{u}{\sqrt{n}} \text{ if } \forall j, u(D_j) \\ &= \sqrt{u^2(F_c) + u^2(Q_j)} = u. \end{aligned} \quad (8)$$

For  $m$  identical irradiations, the average dose  $\bar{D}$  and its uncertainty  $u(\bar{D})$ , given by equation (9), are deduced from the total averaged doses measured for each irradiation  $i$ , weighted by their respective uncertainties:

$$\bar{D} = \frac{\sum_{i=1}^m \frac{\bar{D}_i}{u^2(\bar{D}_i)}}{\sum_{i=1}^m \frac{1}{u^2(\bar{D}_i)}} \quad u(\bar{D}) = \sqrt{\frac{1}{\sum_{i=1}^m \frac{1}{u^2(\bar{D}_i)}}}. \quad (9)$$

In the current procedure, the dosimeters are immediately withdrawn from the reactor after irradiation and the total integrated doses are read out within the following 24 h, with a negligible fading.

However, as discussed in the next part (Sect. 4), it is possible to implement a new methodology based on the use of optical fibers, providing the opportunity to perform online photon heating measurements during irradiation.

### 3.5 Application of correction factors

In general, the luminescent response  $Q_{n-\gamma}$  of a dosimeter irradiated in a mixed  $n-\gamma$  field is defined in equation (10) as the sum of neutron and photon components, whose contributions to the total signal depend on the sensitivity of the dosimeter to the respective  $n$  and  $\gamma$  fluxes [19]:

$$Q_{n-\gamma} = \eta_n D_n + \eta_\gamma D_\gamma, \quad (10)$$

**Table 3.** Cavity correction factors in aluminum pillboxes ( $Z_{\text{eff}} = 13$ ) encapsulating different types of dosimeters (see [Tabs. 1](#) and [2](#), [Sect. 2.3](#)), calculated with TRIPOLI in the calibration geometry with less than 0.1% statistical error ( $1\sigma$ ).

Dosimeter	TLD-400	TLD-700	PTL-717	OSLD
$Z_{\text{eff}}$	16.3	8.2	8.2	10.2
$F_p$	1.054	1.055	1.057	1.024

**Table 4.** Thermal neutron response factor and relative neutron/photon sensitivity in the epithermal/fast field adopted for the currently used dosimeters (uncertainties given at  $1\sigma$ ) [[16,19–21,38,47](#)].

Dosimeter	$R$ [Gy ( $10^{12}$ n cm $^{-2}$ ) $^{-1}$ ]	$\eta_n/\eta_\gamma$ ( $E_c < E_n < 10$ MeV)
TLD-400	$0.45 \pm 100\%$ [ <a href="#">23</a> ]	$0.288 \pm 60\%$ [ <a href="#">20</a> ]
TLD-700 (0.01% $^6\text{Li}$ )	$1.4 \pm 22\%$ [ <a href="#">38</a> ]	$0.125 \pm 60\%$ [ <a href="#">20</a> ]
GR-207 (0.007% $^6\text{Li}$ )	$1.4 \pm 30\%$ [ <a href="#">16</a> ]	$0.125 \pm 60\%$ [ <a href="#">20</a> ]
PTL-717 (0.05% $^6\text{Li}$ )	$8.7 \pm 20\%$ [ <a href="#">47</a> ]	$0.125 \pm 60\%$ [ <a href="#">20</a> ]
TLD-500/OSLD	$0.35 \pm 100\%$ [ <a href="#">21</a> ]	$0.242 \pm 60\%$ [ <a href="#">21</a> ]

where  $\eta_n$  and  $\eta_\gamma$  are respectively the neutron and photon sensitivities of the dosimeter [in nC mGy $^{-1}$  for TLDs, and counts mGy $^{-1}$  for OSLDs];  $D_n$  and  $D_\gamma$  are respectively the neutron and photon doses integrated by the dosimeter [in mGy].

The photon dose is then given by equation (11), whose terms are clarified below [[6,19](#)]:

$$D_\gamma = \underbrace{\frac{Q_{n-\gamma}}{\eta_\gamma}}_{(i)} - \underbrace{\frac{\eta_n}{\eta_\gamma} D_n}_{(ii)}. \quad (11)$$

– The first term (i) refers to the dosimeter photon sensitivity  $\eta_\gamma$  which is determined through pure  $\gamma$  field calibration according to equation (12):

$$\eta_\gamma = \frac{Q_\gamma}{D_\gamma} = \frac{Q_\gamma}{K_{\text{air}}} \times \frac{K_{\text{air}}}{D_\gamma} = F_c \times F_p, \quad (12)$$

where  $F_c$  is the  $\gamma$  calibration factor (see [Sect. 3.3](#)); and  $F_p$  is the cavity correction factor governing the relationship between the  $K_{\text{air}}$  reference quantity and the photon dose  $D_\gamma$  actually received by the dosimeter, which depends on the dosimeter and pillbox effective atomic numbers ( $Z_{\text{eff}}$ ). This factor is calculated with Monte Carlo simulations in the calibration geometry. [Table 3](#) shows some of the  $F_p$  values calculated in aluminum pillboxes encapsulating different types of dosimeters.

From equations (7)–(12), the photon dose and its uncertainty can be expressed as shown by the following equations (13):

$$D_\gamma = \frac{\bar{D}}{F_p} - \frac{\eta_n}{\eta_\gamma} D_n u(D_\gamma) \\ = \sqrt{\left(\frac{1}{F_p}\right)^2 u^2(\bar{D}) + \left(\frac{\bar{D}}{F_p}\right)^2 u^2(F_p) + u^2\left(\frac{\eta_n}{\eta_\gamma} D_n\right)}. \quad (13)$$

– The second term (ii) corresponds to the effective neutron dose defined in equation (14) as the sum of a thermal neutron contribution and an epithermal/fast neutron contribution, such discrimination being particularly relevant for LiF TLDs due to the large cross-section of thermal neutron capture by  $^6\text{Li}$  ( $\sigma_{\text{th}} = 941$  b):

$$\frac{\eta_n}{\eta_\gamma} D_n = R\phi_{E_n < E_c} + \left(\frac{\eta_n}{\eta_\gamma} D_n\right)_{E_c < E_n < 10 \text{ MeV}}, \quad (14)$$

where  $R$  is the thermal neutron response factor [in mGy cm $^2$ ], increasing with  $^6\text{Li}$  content in the dosimeter;  $\phi$  is the thermal neutron fluence [in  $n_{\text{th}}$  cm $^{-2}$ ];  $E_n$  and  $E_c$  are respectively the neutron energy and the thermal/epithermal cutoff energy [in eV].

In practice, the thermal neutron response factor  $R$  and the relative neutron/photon sensitivity  $\eta_n/\eta_\gamma$  in the epithermal and fast neutron field, as well as their respective uncertainties, are taken from the literature data suitable for the used dosimeters. The currently adopted values are given in [Table 4](#) from references [[16,19–21,23,38,47](#)]. The direct neutron dose  $D_n$  is then calculated in the reactor geometry. As discussed in [Section 2.2](#), the use of  $^7\text{Li}$  and  $^6\text{Li}$ -enriched TLDs calibrated in both  $\gamma$  and neutron fields would permit to experimentally determine the neutron contribution to the total measured dose using the INFN method [[11](#)] (see [Sect. 2.2](#)), that would avoid resorting to literature data whose uncertainties are usually pretty large (see [Tab. 4](#)).

## 4 Feasibility of online nuclear heating measurements: optical fiber dosimetry methods

### 4.1 General comments

The main purposes of online nuclear heating measurements are to access the instantaneous dose rate delivered in the materials subjected to reactor mixed  $n-\gamma$  field, and to measure the delayed photon dose after reactor shutdown.

A promising field of investigation on such measurements relies on the use of optical fibers, whose implementation for online dosimetry revolves around the following two procedures:

- the use of the fiber as a carrier of optical information toward the dosimeter (laser stimulation), and from the dosimeter to the PMT (luminescent response);
- the use of the fiber itself as a dosimeter, whose properties depend on its chemical composition (material, doping).

An overview of the main dosimetry techniques based on optical fiber measurements is provided in the following sections, and the suitability of each of them for online nuclear heating measurements in ZPR is assessed.

## 4.2 Radiation-induced attenuation (RIA)

The RIA dosimetry relies on the darkening properties of silica glasses ( $\text{SiO}_2$ ) subjected to radiation. The radiation-induced defects in the glass structure leads to a darkening of the fiber core, whose intensity can be correlated with the dose received by the glass. When a certain length of fiber is exposed to ionizing radiation, such a darkening causes an optical transmission decrease in the fiber core, that can be measured by connecting both fiber ends respectively to a light source (LED, laser diode) and to a photodiode. The transmitted light decrease is then linked to the integrated dose thanks to a reference precalibrated RIA of the considered fiber type. The main drawback of this technique relates to the strong fading resulting from the thermal instability of radiation-induced defects, many of which can be annealed at room temperature. As shown in Figure 10, the RIA does not depend on the dose rate up to  $50 \text{ Gy s}^{-1}$ , but it decreases when the source wavelength increases, with a strong fall beyond 500 nm [48]. Such dependency is strongly correlated to the glass chemical composition (especially with the presence of doping agents or OH molecules), as shown in Figure 11 [49], so that the fiber sensitivity can be adapted to the radiation field by varying its composition or exposed length, and the light emission wavelength. For instance, in low-dose environment, it is preferable to expose a large fiber length to ionizing radiation and to use a short emission wavelength to improve the measurement sensitivity. Since undoped silica glasses generally exhibit a rather low sensitivity to radiation, this type of fibers is unsuitable for dosimetry applications. It is however quite appropriate for transmission purposes without large losses of optical information by RIA, especially in high-dose environment such as nuclear reactors. One of the first RIA systems was embedded on the NTS-2 satellite to measure dose rate variations of 0.09 to  $0.25 \text{ Gy day}^{-1}$  within the outer Van Allen belt (see Sect. 2.4), correlated with sunspots activity [50]. RIA dosimetry was then developed in high-energy physics and nuclear applications, as well as in medical physics for the online dose monitoring during radiation treatments (with a 2% accuracy on a total measured dose of about 1 Gy).

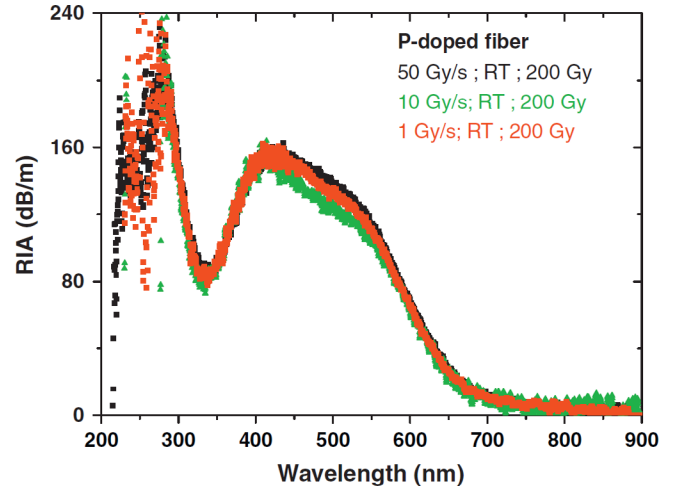


Fig. 10. RIA spectra of P-doped fibers irradiated with 10 keV X-rays at different dose rates up to 200 Gy [48].

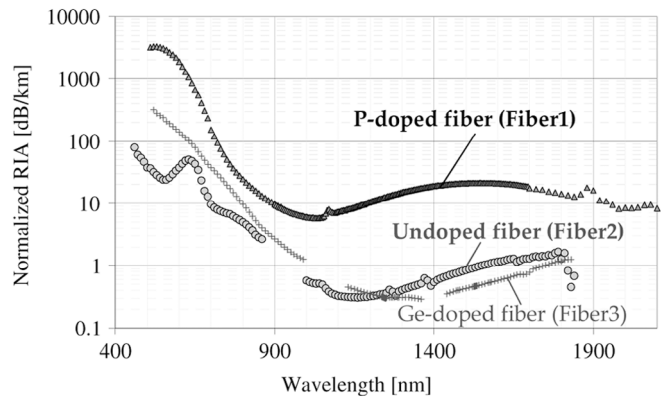
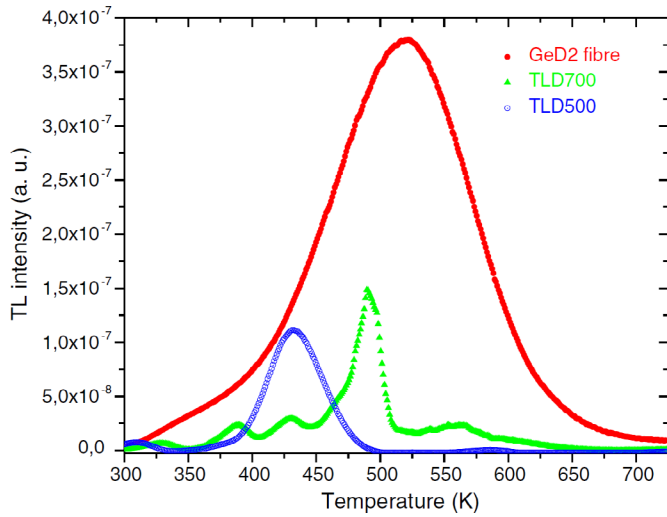


Fig. 11. Comparison of normalized RIA spectra after photon irradiation ( $^{60}\text{Co}$  source) for P-doped fiber (5 Gy), Ge-doped and undoped fibers (100 Gy) [49].

## 4.3 Thermoluminescent dosimetry

A remote thermoluminescent dosimetry system consists of a TLD pellet specifically designed to be connected at the end of an optical fiber [51]. Immediately after irradiation, a focused laser beam provides the thermal stimulation to the TLD, whose luminescent response is redirected through the fiber to the PMT. The opposite face of the TLD is coated with a thin layer of absorbent material intended to reduce heat losses. An air gap may also be inserted between the TLD and the fiber end in order to thermally insulate the latter from the heated TLD. A laser power of 0.4 W is sufficient to locally reach heating rates of several hundreds of  $\text{K s}^{-1}$ , thus optimizing the signal to noise ratio of the measurement by stimulating very quickly the TL response of the dosimeter. In the frame of medical applications, this technique achieved about 1% accuracy above 1 Gy, and 5% for a measured dose of 10 mGy. Furthermore, since the sensitivity of the dosimeter remains high up to 200 m from the laser source and the PMT, the remote TLD is suitable for environmental monitoring, particularly for in



**Fig. 12.** Comparison of the glow curves of GeD2 fiber, TLD-700 and TLD-500 irradiated and read out in the same experimental conditions [52].

situ radiological control of contaminated groundwater. Researchers from LPMC<sup>14</sup> recently explored the TL properties of Ge-doped fibers previously stripped of their polymer sheath (caution related to the fiber heating) and then irradiated with X-rays [52]. It has been shown that such type of fiber, used itself as a dosimeter, fulfills the TL characteristics required by medical dosimetry, such as high sensitivity and dynamic range, and low dependency on the dose rate. In particular, Figure 12 illustrates the high sensitivity of Ge-doped fibers by comparing the GC of a GeD2 fiber with those of LiF and alumina TLDs (respectively TLD-700 and TLD-500), whose fading properties are equivalent when handled away from light sources. The Ge-doped fiber heating law is quite simple and, unlike for usual TLDs, there is no need to anneal the fiber to regenerate it. In addition, its sensitivity increases with heating rate, so that this technique suits the routine measurements in the medical field. However, remote TL measurement technique may be unsuitable for reactor dosimetry because of the safety constraints related to the insertion of an in-core heating source.

#### 4.4 Radioluminescent dosimetry

When subjected to ionizing radiation, optical fibers produce a prompt luminescence called radioluminescence (RL) related to the presence of defects and chemical impurities within silica glasses. Such luminescence is emitted during irradiation without any stimulation, and it is notably enhanced by rare earths doping (Ce, Sm). In general, the RL intensity of an irradiated glass is proportional to the dose rate, thus allowing real-time measurement of the dose rate during irradiation. At low wavelengths, the intensity of RL emission bands is affected by the RIA (see Sect. 4.2), thereby reducing the linearity range of the fiber RL response. This

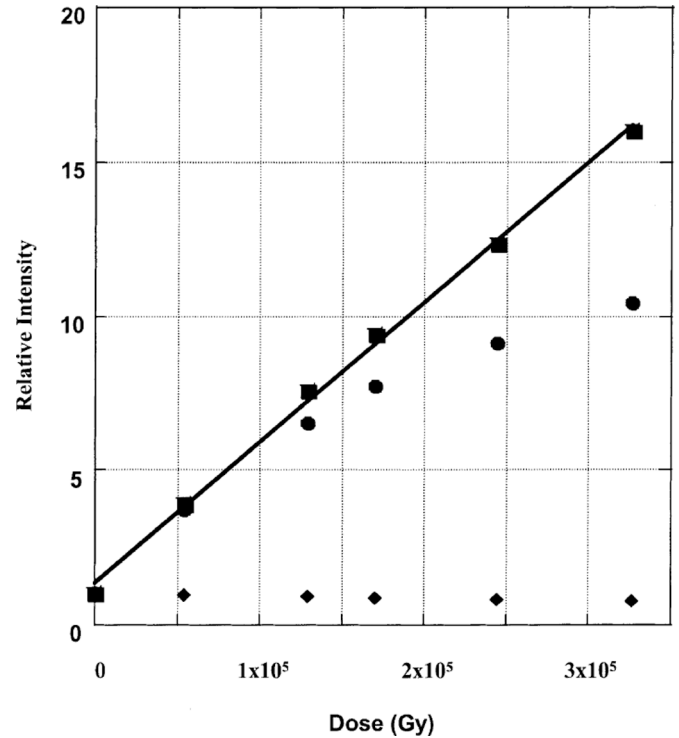


**Fig. 13.** Relative intensity of the two RL bands (circles and diamonds) of an undoped silica fiber irradiated with 40 keV X-rays as a function of the cumulative dose (the squares refer to the corrected intensity for the RIA losses of the RL band symbolized by circles) [53].

effect is illustrated in Figure 13 for the two RL bands (circles and diamonds) of an undoped silica fiber irradiated with 40 keV X-rays [53]. Beyond a cumulative dose around  $10^5$  Gy, the RL intensity has to be corrected for the RIA losses within the fiber core. Such correction allows retrieving the actual RL emission of the fiber at high doses, so as to improve the linearity range of the measurement (see Fig. 13, where the squares refer to the corrected intensity for the RIA losses of the RL band symbolized by circles). A “control” fiber may be used to correct the RL response of the “dosimeter” fiber for spurious signals such as scintillation light and Cerenkov radiation (generally occurring around 1 MeV). Lastly, since RL measurements require a dose rate calibration, it might be difficult to implement this technique for reactor applications, compared with other techniques for which only a dose calibration is needed.

#### 4.5 Optically stimulated luminescent dosimetry

The remote OSLD technique relies on the principle outlined in Section 4.3 related to TL systems, except that the absorbent layer coating is unnecessary in this case [53]. Such online measurement method is particularly appropriate when in situ heating is strictly prohibited (during radiation treatments for instance). The laser stimulation of the OSLD is triggered through the fiber at the end of irradiation, and the luminescent signal is immediately transmitted *via* the fiber to the PMT [54–57]. The OSL emission following a stimulation pulse is very fast, and then

<sup>14</sup> Laboratoire de Physique de la Matière Condensée (Nice, France).

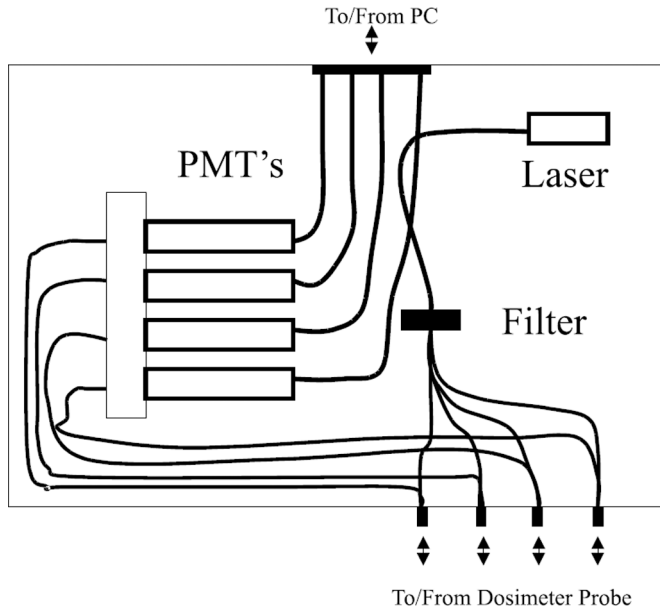


**Fig. 14.** Schematic description of a four-channel online OSL dosimetry system [53].

decreases all the more quickly than the laser power is high. A different approach is to use the fiber itself as an OSL dosimeter. A Cu-doped fused quartz exhibiting outstanding optical, mechanical and dosimetric properties was developed at the NRL<sup>15</sup> and implemented for medical purposes within an online dosimetry system schematized in Figure 14 [53]. Each dosimeter probe consists of a 1 mm length of Cu-doped fiber, 0.4 mm in diameter, spliced to the end of a 1 m long undoped fiber with the same diameter and physical properties. A Teflon sheath insulates the assembly from external light, the radiation-sensitive fiber portion being further coated with a low-refractive index polymer cladding lined with a black enamel coating. The laser stimulation of the four dosimeter probes and their OSL responses are respectively delivered and collected by the PMT's through different fiber bundle arrangements. Using such kind of setup, it may be very interesting to couple the RL and OSL remote dosimetry techniques, according to the following two stimulation protocols [58], which are also illustrated in Figure 15:

- Online RL measurements with post-irradiation OSL stimulation: the RL signal emitted by the dosimeter under irradiation (see Sect. 4.4) is acquired in real time at a rate of 10 to 100 readouts per second. Knowing the initial RL sensitivity of the dosimeter and its dependence upon the total absorbed dose<sup>16</sup>, one can estimate the latter through iterative sensitivity corrections. Immediately after drop of the control rods, the laser stimulation is triggered so as to acquire the OSL response of the dosimeter, which is directly proportional to the total

absorbed dose. Unlike online RL measurements, post-irradiation OSL measurements are not affected by spurious signals (scintillation, Cerenkov), that makes possible to quantify those signals by subtracting the total doses derived from online RL (integral) and post-irradiation OSL measurements.

- Online RL measurements with periodic OSL stimulations: in addition to real-time acquisition of the RL signal, a laser pulse is used to periodically stimulate the dosimeter, whose OSL response is extracted from RL and scintillation/Cerenkov background by subtracting two consecutive periods respectively acquired with and without laser stimulation. The periodic stimulation of the OSLD during irradiation induces two antagonistic processes: the amount of trapped electrons within the gap increases due to radiation effects, while a part of them is released at each laser pulse [58]. Thus, the OSL signal acquired during the  $n$ th laser stimulation must be corrected for the fraction of electrons released during the  $(n-1)$  previous stimulation periods, according to equation (15):

$$\text{OSL}'(n) = \text{OSL}(n) + \sum_{i=1}^{n-1} \text{OSL}(i)F_D(i), \quad (15)$$

where  $\text{OSL}'(n)$  and  $\text{OSL}(n)$  are respectively the corrected and uncorrected intensities of the OSL signal acquired during the  $n$ th laser stimulation;  $\text{OSL}'(i)$  is the uncorrected intensity of the OSL signal acquired during the  $i$ th stimulation; and  $F_D(i)$  is the depletion factor related to the fraction of electrons released during the  $i$ th stimulation, estimated from the shape of the  $i$ th OSL signal.

The implementation of one protocol rather than another is mainly dictated by the stimulation time needed to satisfactorily extract the OSL signal, that depends on the probe material and dimensions, as well as on the laser beam power. Finally, thanks to an optimization of the OSL stimulation protocol, it may be potentially feasible to assess the instantaneous dose rate during irradiation, as well as the delayed photon dose after reactor shutdown.

## 5 Intercomparison of dosimetry techniques: suitability for photon heating measurements in ZPR

Table 5 provides an intercomparison of the previously described dosimetry techniques from the point of view of their suitability for post-irradiation and/or online photon heating measurements in ZPR. Some insights from ongoing developments and potential further improvements are given in this table.

## 6 Conclusions and experimental outlook

As part of an instrumental optimization approach currently in progress at CEA Cadarache, this article provides a bibliographical overview of the methodological issues related to the photon heating measurement

<sup>15</sup> Naval Research Laboratory (Washington DC, US).

<sup>16</sup> The RL sensitivity increases with the total absorbed dose, such dependency being assessed through dosimeter precalibration.

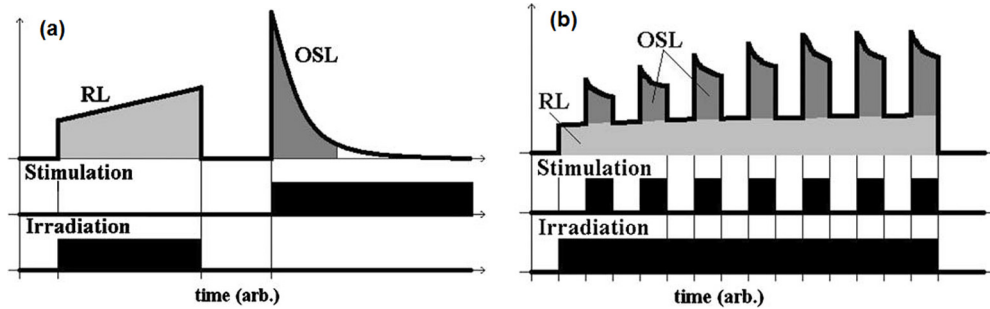


**Fig. 15.** Diagrams of the remote RL/OSL measurement protocols with post-irradiation (a) and periodic (b) OSL stimulations [58].

**Table 5.** Suitability, ongoing developments and potential further improvements of the different dosimetry techniques for post-irradiation and/or online photon heating measurements in ZPR.

Measurement technique	Dosimetry in ZPR	Comments/ongoing developments and further improvements
Post-irradiation	TLD ✓	– Need to experimentally determine the neutron contribution to the total measured dose, by using the discrimination method described in Section 2.2 [11,59]. – A newly developed measurement method in high and ultra-high dose environments (fission and fusion power facilities, MTR, high-energy research accelerators, emergency dosimetry, etc.) could be used to measure doses up to kGy or MGy [60–62].
	OSLD ✓	– Linearity range limited to a few Gy [22], hence leading to a rapid saturation of the dosimeter when it is merely partially emptied at each readout.
Online (optical fiber)	RIA ✗	Requires dose rate calibration and correction for the RIA losses beyond $10^5$ Gy [53].
	TL ✗	
	RL ✓	
	OSL ✓	The probe geometry, as well as the light source power and the stimulation protocol, have to be adapted to reactor specifications and irradiation parameters (time, operating power, dose rate), so as to ensure the online acquisition of the OSL signal without saturating the detector [58,63]. Using RL emission together with OSL signal [55,58], it may be possible to assess the instantaneous dose rate during irradiation and after reactor shutdown (delayed photons).

techniques in low-power research reactors (ZPRs). The main conclusions and experimental outlook can be summarized as follows:

Within the last few decades, luminescent dosimetry techniques have been developed in many application fields such as medical physics (radiation treatments, imaging), personal and environmental monitoring, on-board space systems, high-energy physics (characterization of particle beams) and nuclear energy (power plants, research reactors). The most commonly used dosimeters for such applications are doped-fluoride based TLDs (LiF:Mg,Ti, LiF:Mg,Cu,P, CaF<sub>2</sub>:Mn) and alumina OSLDs (Al<sub>2</sub>O<sub>3</sub>:C), whose dosimetric properties have been widely investigated in terms of sensitivity, repeatability, reproducibility, spectral emission, etc. The successive improvements implemented during the photon heating measurement campaigns conducted in ÉOLE and MINERVE critical

mock-ups at CEA Cadarache have led to the currently used methodology, providing a quite good reproducibility with reduced uncertainties (less than 10% at  $1\sigma$ ) and optimized C/E ratios (0.80 to 1.04). This methodology requires a sufficiently large thickness of surrounding material (pill-box) to achieve CPE within the encapsulated TLDs and OSLDs, those being precalibrated in pure  $\gamma$  field (<sup>60</sup>Co source). Irradiations are then performed in ZPR mixed  $n$ - $\gamma$  field on constant power levels with divergence dose subtraction and background noise correction. Finally, the determination of integrated doses implies a processing of raw measurements thanks to calibration and cavity correction factors, as well as neutron dose correction, which is currently deduced from literature data with pretty high uncertainties (up to 100% at  $1\sigma$ ). Starting from that current methodology, one can identify some optimization opportunities revolving around the following three aspects:

- The determination of neutron contribution to the total measured dose remains a key point of photon heating measurements in ZPR. A promising method based on the use of LiF TLDs enriched with  $^7\text{Li}$  and  $^6\text{Li}$ , precalibrated both in photon and neutron fields, has been recently developed at INFN for medical purposes, aiming at deconvoluting the GC of TLDs irradiated in mixed  $n$ - $\gamma$  field, from the peak heights measured on the photon and neutron calibration GCs. Such deconvolution processing would allow to experimentally discriminate the photon and neutron components of the total measured dose, without resorting to literature data. Preliminary tests are currently being designed at CEA Cadarache and LPSC<sup>17</sup> to assess the applicability of this method to photon heating measurements in ZPR, in particular regarding the calibration phase in pure neutron field.
- The current methodology relies on a post-irradiation readout about 24 h after withdrawal of dosimeters from reactor. Nevertheless, it would be very advantageous to perform online photon heating measurements by implementing a fibered setup, that would primarily avoid instrumental constraints related to the immediate withdrawal of dosimeters after irradiation. In practice, the remote RL/OSL technique seems to be the most appropriate method for photon heating measurements in ZPR. Such kind of setup relies on the following principle : a laser stimulation is guided into an optical fiber at the end of which an OSLD is connected, while the RL and/or OSL responses of the irradiated dosimeter are remotely read out through the same fiber or another. Thanks to a dosimeter probe and a fiber design adapted to ZPR requirements, the OSL stimulation protocol could be optimized so as to measure either instantaneous dose rates during irradiation or delayed photon doses after reactor shutdown. Feasibility experiments have been recently undertaken in ÉOLE reactor, using an OSL/optical fiber coupling system developed in the past few years at CEA Saclay, initially for medical applications.
- The use of the luminescent dosimetry techniques in high-dose environments (power reactors, irradiation facilities, etc.) is generally prohibited by the saturation of the dosimeters beyond a few Gy for OSLDs or tens of Gy for TLDs. However, some ongoing developments on the use of TLDs and fibered OSLDs in high and ultra-high dose environments (not presented in this paper) could allow bypassing this issue.

At last, we remind that nuclear heating measurements in ZPR are implemented to contribute to the validation of neutron and photon calculation schemes, which are developed in the frame of the design studies for future power and research reactors. This article is primarily focused on the technical and experimental issues related to the nuclear heating prediction. But obviously, the evaluation of the calculation schemes (MCNP, TRIPOLI) and the

feedback on the associated nuclear data (ENDF, JEFF) are mandatory to improve the C/E ratios. Thus, optimization studies are jointly led on experimental and calculation aspects.

## References

1. A. Lyoussi, *Détection de rayonnements et instrumentation nucléaire* (EDP Sciences, Les Ulis, France, 2010)
2. C. Reynard-Carette, J. Brun, M. Carette, M. Muraglia, A. Janulyte, Y. Zerega, J. André, A. Lyoussi, G. Bignan, J.-P. Chauvin, D. Fourmentel, C. Gonnier, P. Guimbal, J.-Y. Malo, J.-F. Villard, *RRFM-IGORR, Prague, Czech Republic* (2012)
3. F.H. Attix, *Introduction to radiological physics, radiation dosimetry* (Wiley, New York, USA, 1986)
4. D. Fourmentel, P. Filliatre, J.-F. Villard, A. Lyoussi, C. Reynard-Carette, H. Carcreff, *Nucl. Instrum. Methods Phys. Res., Sect. A* **724**, 76 (2013)
5. D. Lapraz, P. Iacconi, *Radioprotection* **25**, 117 (1990)
6. P. Blaise, J. Di Salvo, C. Vaglio-Gaudard, D. Bernard, H. Amharrak, M. Lemaire, S. Ravaux, *Phys. Proc.* **59**, 3 (2014)
7. E.G. Yukihara, S.W.S. McKeever, *Optically stimulated luminescence: fundamentals and applications* (Wiley, West Sussex, UK, 2011)
8. V. Kortov, *Radiat. Meas.* **42**, 576 (2007)
9. R.H. Thomas, *Advances in radiation protection and dosimetry in medicine* (Springer, New York, USA, 1980)
10. A. Ismail, J.-Y. Giraud, G.N. Lu, R. Sihanath, P. Pittet, J.M. Galvan, J. Balosso, *Cancer/Radiothérapie* **13**, 182 (2009)
11. G. Gambarini, G. Bartesaghi, S. Agosteo, E. Vanossi, M. Carrara, M. Borroni, *Radiat. Meas.* **45**, 640 (2010)
12. Saint-Gobain, MCP physical constants: LiF:Mg, Cu, P physical data and constants, 2000
13. Harshaw, Product overview: materials and assemblies for thermoluminescence dosimetry, 2015
14. TLD-Poland, Thermoluminescent detectors, TLD pellets and powders for radiation protection and medical dosimetry (2016), [www.tld.com.pl](http://www.tld.com.pl)
15. China Quartz Technology, LiF for dosimetry data sheet: GR-200, 2003
16. R. Bedogni, A. Esposito, M. Angelone, M. Chiti, *IEEE Trans. Nucl. Sci.* **53**, 1367 (2006)
17. R. Bedogni, M. Angelone, A. Esposito, M. Chiti, *Radiat. Prot. Dosim.* **120**, 369 (2006)
18. G.A. Klemic, N. Azziz, S.A. Marino, *Radiat. Prot. Dosim.* **65**, 221 (1996)
19. H. Amharrak, Ph.D. thesis, Aix-Marseille Université, France, 2012
20. J.A.B. Gibson, *Radiat. Prot. Dosim.* **15**, 253 (1986)
21. G. Portal, Ph.D. thesis, Université Paul Sabatier, France, 1978
22. Landauer, InLight complete dosimetry system solution: nanoDot dosimeter, 2015
23. ASTM, Standard practice for application of  $\text{CaF}_2(\text{Mn})$  thermoluminescence dosimeters in mixed neutron-photon environments, 2011
24. J. Fesquet, D. Benoit, J.-R. Vaillé, P. Garcia, H. Prevost, J. Gasiot, L. Dusseau, *Radioprotection* **41**, 87 (2006)
25. L. Dusseau, D. Plattard, J.-R. Vaillé, G. Polge, G. Ranchoux, F. Saïgne, J. Fesquet, R. Ecoffet, J. Gasiot, *IEEE Trans. Nucl. Sci.* **47**, 2412 (2000)

<sup>17</sup> Laboratoire de Physique Subatomique et de Cosmologie (Grenoble, France).

26. H. Amharrak, J. Di Salvo, A. Lyoussi, M. Carette, C. Reynard-Carette, Nucl. Instrum. Methods Phys. Res. A **749**, 57 (2014)
27. T.K. Wang, F.M. Clikeman, K.O. Ott, Nucl. Sci. Eng. **93**, 262 (1986)
28. A.D. Knipe, R. De Wouters, IAEA report IAEA-SM-244/35, in *International Symposium on Fast Reactor Physics, Aix-en-Provence, France* (1975)
29. G.G. Simons, A.P. Olson, Nucl. Sci. Eng. **53**, 176 (1974)
30. B. Mukherjee, H. Bock, N. Vana, Nucl. Instrum. Methods Phys. Res. A **256**, 610 (1987)
31. E. Gaillard-Lecanu, Q. Chau, F. Tromprier, V.I. Tcvetkov, E.Y. Tarasova, E.D. Klechtchenko, Radiat. Meas. **33**, 859 (2001)
32. F. Tromprier, C. Huet, R. Medioni, I. Robbes, B. Asselineau, Radiat. Meas. **43**, 1077 (2008)
33. J.P. Santos, J.G. Marques, A.C. Fernandes, M. Osvay, Nucl. Instrum. Methods Phys. Res. A **580**, 310 (2007)
34. H. Ait Abderrahim, in *ANS Radiation Protection and Shielding Division Topical Conference, Nashville, Tennessee, US* (1998)
35. D. Calamand, in *NEARCP Meeting, Aix-en-Provence, France* (1984)
36. R. De Wouters, in *International Conference on Physics of Reactors, Marseille, France* (1990)
37. A. Lüthi, Ph.D. thesis, Ecole Polytechnique Fédérale de Lausanne, Switzerland, 1998
38. D. Blanchet, Ph.D. thesis, Université Blaise Pascal, France, 2006
39. D. Blanchet, N. Huot, P. Sireta, H. Serviere, M. Boyard, M. Antony, V. Laval, P. Henrard, Ann. Nucl. Energy **35**, 731 (2008)
40. G. Rimpault, D. Bernard, D. Blanchet, C. Vaglio-Gaudard, S. Ravaux, A. Santamarina, Phys. Proc. **31**, 3 (2012)
41. H. Amharrak, J. Di Salvo, A. Lyoussi, P. Blaise, M. Carette, A. Roche, M. Masson-Fauchier, A. Pepino, C. Reynard-Carette, IEEE Trans. Nucl. Sci. **61**, 2515 (2014)
42. S. Ravaux, Ph.D. thesis, Université de Grenoble, France, 2013
43. A. Santamarina, C. Vaglio-Gaudard, P. Blaise, J-C. Klein, N. Huot, O. Litaize, N. Thiollay, J-F. Vidal, in *International Conference on the Physics of Reactors, Interlaken, Switzerland* (2008)
44. H. Amharrak, J. Di Salvo, A. Lyoussi, A. Roche, M. Masson-Fauchier, A. Pepino, J.C. Bosq, M. Carette, IEEE Trans. Nucl. Sci. **59**, 1360 (2012)
45. E. B. Podgorsak, *Radiation oncology physics: a handbook for teachers and students* (IAEA, Vienna, Austria, 2005)
46. M. Lemaire, Ph.D. thesis, Aix-Marseille Université, France, 2015
47. D. Calamand, Ph.D. thesis, Université de Provence, France, 1978
48. S. Girard, Y. Ouerdane, C. Marcandella, A. Boukenter, S. Quenard, N. Authier, J. Non-Cryst. Solids **357**, 1871 (2011)
49. E. Regnier, I. Flammer, S. Girard, F. Gooijer, F. Achten, G. Kuyt, IEEE Trans. Nucl. Sci. **54**, 1115 (2007)
50. B.D. Evans, G.H. Sigel, J.B. Langworthy, B.J. Faraday, IEEE Trans. Nucl. Sci. **NS-25**, 1619 (1978)
51. S.C. Jones, J.A. Sweet, P. Braunlich, J.M. Hoffman, J.E. Hegland, Radiat. Prot. Dosim. **47**, 525 (1993)
52. M. Benabdesselam, F. Mady, S. Girard, J. Non-Cryst. Solids **360**, 9 (2013)
53. A.L. Huston, B.L. Justus, P.L. Falkenstein, R.W. Miller, H. Ning, R. Altemus, Nucl. Instrum. Methods Phys. Res. B **184**, 55 (2001)
54. G. Ranchoux, S. Magne, J-P. Bouvet, P. Ferdinand, Radiat. Prot. Dosim. **100**, 255 (2002)
55. S. Magne, L. Auger, J-M. Bordy, L. de Carlan, A. Isambert, A. Bridier, P. Ferdinand, J. Barthe, Radiat. Prot. Dosim. **131**, 93 (2008)
56. S. Magne, L. de Carlan, J-M. Bordy, A. Isambert, A. Bridier, P. Ferdinand, IEEE Trans. Nucl. Sci. **58**, 386 (2011)
57. S. Magne, L. de Carlan, A. Bridier, A. Isambert, P. Ferdinand, R. Hugon, J. Guillon, IRBM **31**, 82 (2010)
58. R. Gaza, S.W.S. McKeever, M.S. Akselrod, A. Akselrod, T. Underwood, C. Yoder, C.E. Andersen, M.C. Aznar, C.J. Marckmann, L. Botter-Jensen, Radiat. Meas. **38**, 809 (2004)
59. M. Le Guillou, A. Billebaud, A. Gruel, G. Kessedjian, O. Méplan, C. Destouches, P. Blaise, The CANDELLE experiment for characterization of neutron sensitivity of LiF TLDs, in *ANIMMA conference, Liège, Belgium* (2017), submitted
60. B. Obryk, H.J. Khoury, V.S. Barros, P.L. Guzzo, P. Bilski, Radiat. Meas. **71**, 25 (2014)
61. H.J. Khoury, B. Obryk, V.S. Barros, P.L. Guzzo, C.G. Ferreira, P. Bilski, P. Olko, Radiat. Meas. **46**, 1878 (2011)
62. P. Bilski, B. Obryk, Z. Stuglik, Radiat. Meas. **45**, 576 (2010)
63. K. Ueno, K. Tominaga, T. Tadokoro, K. Ishizawa, Y. Takahashi, H. Kuwabara, IEEE Trans. Nucl. Sci. **63**, 2262 (2016)

**Cite this article as:** Mael Le Guillou, Adrien Gruel, Christophe Destouches, Patrick Blaise, State of the art on nuclear heating measurement methods and expected improvements in zero power research reactors, EPJ Nuclear Sci. Technol. **3**, 11 (2017)